Strong-field approximation for Coulomb explosion of H_2^+ by short intense laser pulses

H. A. Leth,[1] L. B. Madsen,[1] and J. F. McCann[2]

[1]*Lundbeck Foundation Theoretical Center for Quantum System Research, Department of Physics and Astronomy, University of Aarhus, 8000 Århus C, Denmark*

[2]*Centre for Theoretical Atomic Molecular and Optical Physics, School of Mathematics and Physics, Queen's University Belfast, Belfast BT7 1NN, UK*

(Dated: November 24, 2009)

We present a simple quantum mechanical model to describe Coulomb explosion of H_2^+ by short, intense, infrared laser pulses. The model is based on the length gauge version of the molecular strong-field approximation and is valid for pulses shorter than 50 fs where the process of dissociation prior to ionization is negligible. The results are compared with recent experimental results for the proton energy spectrum [I. Ben-Itzhak et al., Phys. Rev. Lett. **95**, 073002 (2005), B. D. Esry et al., Phys. Rev. Lett. **97**, 013003 (2006)]. The predictions of the model reproduce the profile of the spectrum although the peak energy is slightly lower than the observations. For comparison, we also present results obtained by two different tunneling models for this process.

PACS numbers: 32.80.Rm,33.80.Rv,42.50.Hz.

I. INTRODUCTION

Ultrashort, highly-intense, laser pulses at infrared wavelengths are currently being used to study molecular dynamics under extreme conditions. These systems are commonly based upon a Ti:Sapphire laser, tunable around 790 nm, which can reach peak intensities in the range 10^{13}-10^{17} W/cm^2, with pulse lengths shorter than 50 fs. Consequently energy can be deposited on timescales shorter than the fastest molecular vibration with field strengths comparable to the molecular bond. When molecules are exposed to such an environment, the response is highly-nonlinear and generally leads to multiple dissociative ionization and high-order optical scattering. Indeed the multiple fragmentation process for a heavy polyatomic multi-electron system prevents a detailed analysis of the energy transfer, simply due to the proliferation of fragments produced. Small molecular systems, on the other hand, have simpler structure and fewer relaxation channels. Moreover, the fundamental molecules such as H_2 or D_2, have an intrinsic value owing to their fast vibration. Since a 790 nm pulse has a cycle period of 2.6 fs, and perhaps 10-50 fs duration, the vibration provides an additional internal clock that records the response of the electronic excitation during the passage of the pulse. Consequently, there has been extensive study of the interaction of intense field dissociative ionization of H_2 an H_2^+ with progressively shorter and more intense pulses and, in particular, using the ejected proton energy spectrum as an indicator of the electron response and a diagnostic of the pulse itself. For reviews of progress in this field one can consult, for example, Refs. [1, 2, 3].

The effect of the driving pulse on the rates of dissociation and ionization as well as the energy of the fragments has been discussed in Refs. [4, 5]. It has been noted that the kinetic energy release (KER) spectra indicated a decrease in energy of the ionization products when the pulse duration was increased [6]. For a, comparatively long, 90 fs pulse, the observation of a proton energy peak near 2 eV would correspond to an internuclear separation $R \sim 7$ a_0 at the instant of ionization. Given the equilibrium bond length of H_2^+ is $R = 2$ a_0, this suggests dissociation occurring prior to ionization. The increased probability of ionization with increasing R can be understood by the mechanism of resonantly-enhanced multiphoton ionization via the antibonding $2p\sigma_u^+$ state [7, 8] when the resonances are tuned 'from the red' as the bond expands. Conversely, at very high intensities the ionization process can be characterized as a tunneling transition. The associated shape resonances of the molecular ion produce the effects known as charge-resonance enhanced ionization [9] and dynamic tunneling ionization [10]. These ionization mechanisms, diabatic (multiphoton) and adiabatic (tunneling) ionization, can be studied indirectly via the proton emission spectrum.

Perhaps the most interesting aspect of current experiments is that the laser intensities are high enough to explore the adiabatic and diabatic regimes, and also pulse durations are short enough to probe the vibrational motion. The study of bond-stretching during the ionization process has been made possible by enhanced control over pulse duration [4, 11] and through pump-probe techniques [12, 13, 14]. In Ref. [13] it was shown that if H_2 was subjected to two ultra-short pulses, the relative yield of low-energy protons raised at a probe delay of 24 fs. Similar evidence for dissociation prior to ionization was reported in Ref. [7] using single 100 fs pulses on a H_2^+ target. In this case, the KER-spectrum was explained by one- or two-photon absorption to the dissociation channel followed by ionization at a separation of 12 a_0 giving a structure reflecting the initial distribution of vibrational states. All of these experiments resulted in a maximum kinetic energy of the protons in the order of 4 eV.

To minimize the effect of dissociation and thereby be able to observe protons with higher energies, shorter pulses are needed. Experiments using 45 fs pulses showed KER-spectra in the range of 2-10 eV when the intensity

exceeded 1.7×10^{14} W/cm^2 [4, 11, 15]. At lower intensities the dissociation channel dominated completely and no Coulomb explosion was observed. The structure of these spectra was very recently qualitatively explained by associating the critical bond lengths with the Floquet (dressed) state [15] crossing with the ionic $(1/R)$ curve. The underlying physical reason is that the density of states is very high at threshold and there will be a resonant coupling to a quasi-continuum. The strength and width of the peaks are partly restricted by the number of photons involved, and whether or not the pulse is long enough for the molecular expansion to occur, and so reach the crossing before the pulse ends. Using this model, and fitting a 12-parameter function, gives very good agreement with the observations.

In this work we present a simple quantum mechanical model designed to predict the high-energy part of the KER-spectrum of dissociative ionization of H_2^+. We use the strong-field approximation (SFA) within the length gauge [16, 17]. That is we calculate transition rates from a molecular state, in which the laser field is neglected, to a state in which the laser field is accounted for to all orders, but some approximations are made for the three-body continuum. The calculations are simplified by assuming the Born-Oppenheimer separation of motions, and the Franck-Condon principle is invoked for the nuclear motion. These approximations allow us to determine the dissociative ionization *rates* to different channels in a simple way. The pulse is presented by a Fourier expansion so that the temporal intensity variation is taken into account. This averaging is important due to the ponderomotive shift of the electron which may cause channel closings when the intensity is raised.

Following this procedure, and integrating over the electron spectrum, the proton energy distribution can be obtained. Comparing with recent experiments [4, 15], we find the model predictions to be in very good qualitative agreement for the shape of the distribution. However, our calculations predict the peak of the proton spectrum at slightly lower energies than that observed in experiment. Finally, for completion, we compare the predictions of our model with tunneling theory calculations. Atomic units ($|e| = \hbar = m_e = a_0 = 1$) are used throughout unless indicated otherwise.

II. MODEL

We consider the transition from an initial field-free state to a state in which the electron is only affected by the laser light, and the two protons are only subject to their mutual Coulomb repulsion. There are three essential elements of the model. Firstly, the initial state, in which the vibrational population distribution plays a key role. Secondly, the overlap of these vibrational states with the final Coulomb states of the proton pair is of great importance in modulating the proton spectrum. Thirdly, and most importantly, the coupling to the continuum, the nonpertubative photoionization rate, as a function of bond length and laser intensity will determine the range of proton energies. All three factors are intrinsically linked.

Consider a monochromatic plane-wave component of the light field, with linear polarization, $\hat{z}$, and angular frequency ω so that the vector potential in the dipole-approximation is

$$\boldsymbol{A}(t) = A_0 \hat{z} f(t) \cos\omega t \ , \tag{1}$$

where A_0 is the field amplitude, and the pulse shape is described by the factor, $0 \le f(t) \le 1$, which we take to be a Gaussian profile.

A. Molecular states

The process of formation of H_2^+, requires ionization of the neutral species. The molecular ion H_2^+ has only a single bound electronic state $(1s\sigma_g)$ that is exactly known. The nuclear relaxation that follows this primary ionization is not so well defined and remains a source of uncertainty and investigation [2]. Nonetheless, to a very good approximation, the rotational degrees of freedom can be considered as frozen since its characteristic timescale of ~ 170 fs is much longer than the pulse duration. However, this results in an ensemble of vibrational modes, as observed in experiment [18]. As usual, the z-axis of the laboratory reference frame is defined by the polarization vector, while the z-axis of the molecular (body-fixed) frame is defined by the internuclear axis. The notation for the coordinates is that $\boldsymbol{R}$ denotes the internuclear vector and the electron coordinate with respect to the internuclear midpoint, is denoted by $\boldsymbol{r}$. In the following presentation, for consistency, the laboratory reference frame is employed. If we let ν denote the vibrational quantum number, then the eigenstates of the initial ensemble can be expressed as:

$$\Psi_{i\nu}(\boldsymbol{R}, \boldsymbol{r}, t) = \phi_i(\boldsymbol{r}, \boldsymbol{R}) \chi_{i\nu}(R) e^{-iE_{i\nu}t}, \tag{2}$$

where $\phi_i(\boldsymbol{r}, \boldsymbol{R})$ is the electronic wave function, with energy $\varepsilon_i(R)$, and $\chi_{i\nu}(R)$ is the vibrational eigenfunction with eigenvalue $E_{Ni\nu}$. The total energy is then, $E_{i\nu} = \varepsilon_i(R_0) + E_{Ni\nu}$. Recall that the electronic function has a σ_g^+ symmetry, and the transformation of $\phi_i(\boldsymbol{r}, \boldsymbol{R})$ from laboratory to molecule frame is effected by the Wigner D rotation matrix [19].

In the final state, given the large separation between the nuclei and the electron at the time of ionization, we suppose that the influence of the protons on the electron is negligible compared to that of the external field [17]. This is consistent with the asymptotic ($t \to +\infty$) limit of the system as a (decoupled) product state of an outgoing Volkov wave ϕ_f (electron in the electromagnetic field) and a Coulomb wave χ_f for the proton motion:

$$\Psi_f(R, \boldsymbol{r}, t) = \phi_f(\boldsymbol{r}, t) \chi_f(R, t). \tag{3}$$

For an electron in a laser field described by (1), the length-gauge Hamiltonian is given by

$$H_f^{elec} = \frac{1}{2}p^2 + \boldsymbol{r}\cdot\boldsymbol{F}, \tag{4}$$

where $\boldsymbol{p}$ is the canonical momentum and, $\boldsymbol{F} = -\partial_t \boldsymbol{A}$, represents the electric field. The Volkov states form a complete set of solutions to the equation $H_f^{elec}\phi_f(\boldsymbol{r},t) = i\partial_t\phi_f(\boldsymbol{r},t)$ and can be written:

$$\phi_f(\boldsymbol{r},t) = \exp\left[i(\boldsymbol{q}+\boldsymbol{A}(t))\cdot\boldsymbol{r} - i\int_{-\infty}^{t}\frac{(\boldsymbol{q}+\boldsymbol{A}(t'))^2}{2}dt'\right], \tag{5}$$

where $\boldsymbol{q}$ is the kinematic momentum corresponding to a drift energy $q^2/2$, and we denote the ponderomotive energy as $U_p = A_0^2/4$.

Since vibrational energies are much larger than rotational energies, and Coriolis coupling can be neglected at these energies, we make the usual assumption that the proton ejection occurs along the internuclear axis direction without rotation: the axial recoil approximation. Thus, the nuclear motion is governed by the one-dimensional Coulomb repulsion:

$$H_f^{nucl} = -\frac{1}{2\mu}\frac{\partial^2}{\partial R^2} + \frac{1}{R}, \tag{6}$$

where $\mu = \frac{1}{2}m_p$ is the reduced mass. The corresponding eigenfunction, with energy E_{Nf}, and wavenumber, $k_f = \sqrt{2\mu E_{Nf}}$, has the form,

$$\chi_f(R) \;= \sqrt{\tfrac{2\mu}{\pi k_f}}F_0(\tfrac{\mu}{k_f};k_fR), \tag{7}$$

where

$$F_0(\frac{\mu}{k_f};k_fR) = \exp\left(-\frac{\pi}{2}\frac{\mu}{k_f}+ik_fR\right)\left|\Gamma\left(1+i\frac{\gamma}{k_f}\right)\right|k_fR \times{}_1F_1(1+i\frac{\mu}{k_f};2;-2ik_fR), \tag{8}$$

and ${}_1F_1$ is the confluent hypergeometric series. Since the Volkov wave represents all orders of the field amplitude, the final state is a coherent sum of the full spectrum of photoelectron harmonics, including the angular distribution. Since our primary interest here is the comparison with experiment for the proton energy spectrum, we do not present results for the photoelectron differential yields. Instead we must integrate over these degrees of freedom. Furthermore, the initial vibrational state is a mixed state and the orientation of the molecule is random. In all, this amounts to integrating over four continuous variables and summing over two discrete variables, in addition to the matrix element calculation. However, since numerical quadrature is inherently a set of independent calculations, these calculations can readily be performed on a parallel computer.

B. Transition rates

To derive the expression for the transition amplitude, we follow the procedure of Ref. [20], and generalize to the case of an incoherent mixture of initial vibrational states each populated with probability P_ν, defined by the Franck-Condon factors. In this way we obtain the rate w for a transition into the final state Ψ_ν of Eq. (3).

$$w = \sum_\nu P_\nu \sum_{n=n_0}^{\infty} 2\pi\delta(E_f - E_{i\nu} - n\omega)\left|A_{\nu n}\right|^2, \tag{9}$$

where

$$A_{\nu n} = \frac{1}{T}\int_0^T \langle\Psi_f\left|\boldsymbol{r}\cdot\boldsymbol{F}\right|\Psi_{i\nu}\rangle\, dt, \tag{10}$$

and the minimum number of photons absorbed, n_0, is determined by energy conservation. For a given number of absorbed photons, n, the electron momentum is defined as:

$$q = \sqrt{2(E_{i\nu} + n\omega - U_p - E_{Nf})}. \tag{11}$$

To obtain the dissociative ionization rate, we multiply by the density of states per unit energy, per unit solid angle. Using the normalization convention defined above, the appropriate factor is $(2\pi)^{-3}qd^2\hat{\boldsymbol{q}}$. So that we have:

$$\frac{dw}{dE_{Nf}} = \sum_\nu P_\nu \int d\hat{\boldsymbol{q}} \sum_{n=n_0}^{\infty}\frac{q}{(2\pi)^2}\left|A_{\nu n}\right|^2, \tag{12}$$

where $d\hat{\boldsymbol{q}}$ defines the direction of the outgoing electron.

The calculation of $A_{\nu n}(\boldsymbol{q})$ is significantly simplified in the Franck-Condon approximation, where it is assumed that the electronic transition appears almost instantaneously compared to changes in the nuclear position. That is, we can make the integration over the electron coordinate independent of the nuclear coordinate by replacing R by some fixed value R_0,

$$A_{\nu n} = S_{fi}\frac{1}{T}\int_0^T D_{el}(\boldsymbol{R}_0,t)e^{i(E_{Nf}-E_{i\nu})t}dt, \tag{13}$$

where the Franck-Condon factor S_{fi} and the electronic matrix element $D_{el}(\boldsymbol{R}_0,t)$ is given by

$$S_{fi} = \int_0^\infty \chi_f^*(R)\chi_{i\nu}(R)dR, \tag{14}$$

$$D_{el}(\boldsymbol{R}_0,t) = \int \phi_f^*(\boldsymbol{r},t)\boldsymbol{r}\cdot\boldsymbol{F}\phi_i(\boldsymbol{r},\boldsymbol{R}_0)d^3\boldsymbol{r}. \tag{15}$$

We have tested the validity of the Franck-Condon approximation and found it to be accurate, especially for small ν.

The evaluation of the matrix element is conveniently carried out in spherical coordinates [17]. The first step is

to rewrite the expression as

$$D_{el}(\boldsymbol{R}_0,t)=\left(E_{i\nu}-E_{Nf}-\frac{(\boldsymbol{q}+\boldsymbol{A})^2}{2}\right) \times\exp\left[i\int_{-\infty}^{t}\frac{(\boldsymbol{q}+\boldsymbol{A}(t'))^2}{2}dt'\right]\tilde{\phi}_{i\nu}(\boldsymbol{q}+\boldsymbol{A},\boldsymbol{R_0}), \tag{16}$$

where we have used

$$-i\frac{\partial\phi_f^*}{\partial t}=\left[\frac{p^2}{2}+\boldsymbol{r}\cdot\boldsymbol{F}\right]\phi_f^*, \tag{17}$$

and $\tilde{\phi}_i$ denotes the Fourier transform of the electronic wave function,

$$\tilde{\phi}_i(\boldsymbol{k},\boldsymbol{R_0})=\int\exp\left[-i\boldsymbol{k}\cdot\boldsymbol{r}\right]\phi_i(\boldsymbol{r},\boldsymbol{R_0})d^3\boldsymbol{r}. \tag{18}$$

Here $\boldsymbol{k}=\boldsymbol{q}+\boldsymbol{A}$. In the length gauge formulation of the SFA, the transition amplitude only depends on the asymptotic form of the coordinate space initial electronic state [16, 17, 20, 21]. In the laboratory fixed frame this electronic wave function for nuclear orientation $\boldsymbol{R}_0$ reads

$$\phi_i(\boldsymbol{r},\boldsymbol{R_0})=\ r^{(\frac{2}{\kappa}-1)}\exp\left(-\kappa r\right)\sum_l\sum_m C_{l0}D^{(l)}_{m0}(\hat{\boldsymbol{R}}_{\boldsymbol{0}})Y_{lm}(\hat{r}), \tag{19}$$

with C_{l0} asymptotic expansion coefficients [22], and

$$\kappa=\sqrt{2\left(\frac{1}{R_0}-\epsilon_i\right)}, \tag{20}$$

where ϵ_i is the eigenvalue of the electronic Hamiltonian including the nuclear repulsion. In Eq. (19) $D^{(l)}_{m0}(\hat{\boldsymbol{R}}_{\boldsymbol{0}})$ is the Wigner rotation function that effectuates the transformation from the molecular to the laboratory fixed frame.

Finally the electronic matrix element can be found as

$$\begin{aligned}D_{el}(\boldsymbol{R}_0,t)=&\left(E_{i\nu}-E_{Nf}-\frac{(\boldsymbol{q}+\boldsymbol{A})^2}{2}\right)\\&\times\exp\left[i\int_{-\infty}^{t}\frac{(\boldsymbol{q}+\boldsymbol{A}(t'))^2}{2}dt'\right]\\&\times 4\pi\sum_l\sum_m(-i)^l C_{l0}D^{(l)}_{m0}(\hat{\boldsymbol{R}}_{\boldsymbol{0}})\ Y_{lm}(\hat{k})\\&\times\int_0^\infty j_l(kr)r^{(\frac{2}{\kappa}-1)}\exp\left(-\kappa r\right)r^2dr.\end{aligned} \tag{21}$$

The radial integral has a closed analytic form in terms of Gauss's hypergeometric function [23]. The time-integration is performed numerically, along with the sum over the number of photons. In the experimental spectra, the protons resulting from dissociative ionization are collected over a range of ejection angles, with respect to the polarization direction. Averaging over the different orientations of the molecular axis is equivalent, within the axial-recoil model, to summing over the ejected proton directions described by the rotation matrices. This finally reduces to an energy-differential electronic rate, $\Gamma_\nu(E_{Nf})$,

$$\begin{aligned}\Gamma_\nu(E_{Nf})=&q\int d\hat{\boldsymbol{q}}\sum_{n=n_0}^{\infty}\frac{1}{(2\pi)^2}\\&\times\left|\frac{1}{T}\int_0^T D_{el}(R_0,t)e^{i(E_{Nf}-E_{i\nu})t}dt\right|^2.\end{aligned} \tag{22}$$

To obtain the total rate we use Eqs. (12)-(13), i.e., we multiply by the Franck Condon factor

$$\frac{dw_\nu}{dE_{Nf}}=|S_{fi\nu}(E_{Nf})|^2\Gamma_\nu(E_{Nf}) \tag{23}$$

and sum over the different initial states

$$\frac{dw}{dE_{Nf}}=\sum_\nu P_\nu\frac{dw_\nu}{dE_{Nf}}. \tag{24}$$

The values of P_ν are determined by the formation mechanism of the ion. In the context of recent experiments [4, 15] it is reasonable to assume this to be a Franck-Condon distribution.

Finally, to compare with experimental data, we average over the pulse profile, $f(t)$ [Eq. (1)], which is taken to have a Gaussian profile with FWHM 45 fs. Under the assumption that the variation in the pule envelope is slow compared with the optical period, the definition of ionization rate for fixed A_0 is still valid. The ionization process can be significant for intense pulses, and thus we should allow for depletion of the molecular state. To model this process, the total ionization probability is found by integrating this rate over time

$$P_I(E_{Nf})=\sum_\nu\int_{-\infty}^{\infty}\frac{dw_\nu(t)}{dE_{Nf}}N_\nu(t)dt. \tag{25}$$

Here $N_\nu(t)$ denotes the population in a given vibrational state ν. This population can be found from the rate equation:

$$\frac{dN_\nu(t)}{dt}=-\Gamma^\nu_{tot}N_\nu(t), \tag{26}$$

with the boundary condition $N_\nu(-\infty)=P_\nu$ and Γ^ν_{tot} denoting the total rate of ionization from the vibrational state ν. By integrating the differential rate over all final states this rate is found as

$$\Gamma^\nu_{tot}=\int_0^\infty\frac{dw_\nu(t)}{dE_{Nf}}dE_{Nf}. \tag{27}$$

III. RESULTS

In panels (a) and (c) of Fig. 1 we show the predicted KER-spectra for Coulomb explosion of H_2^+ for two pulses

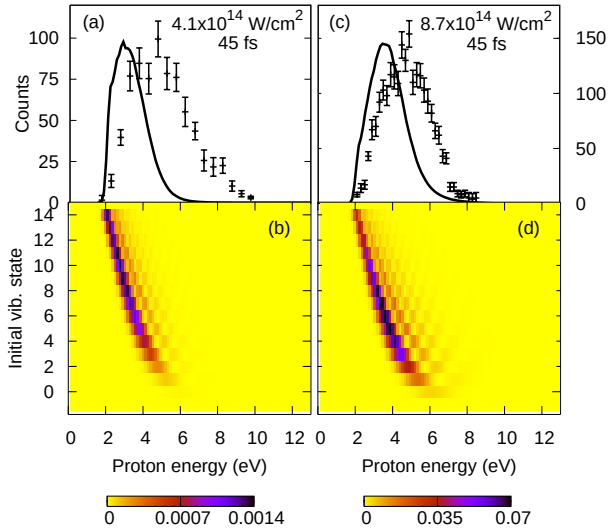

FIG. 1: The predicted KER-spectrum for pulses characterized by a wavelength of 790 nm, a duration of 45 fs (FWHM) and a peak intensity of 4.1×10^{14} W/cm^2 (a) and 8.7×10^{14} W/cm^2 (c). We also plot the experimental results obtained with these pulses in [4] (panel (a)) and [15] (panel (c)), respectively. Panels (b) and (d) show the contributions to the overall spectrum from the different initial vibrational states. The darker the shading the larger the contribution to a given final proton energy from a particular initial vibrational level.

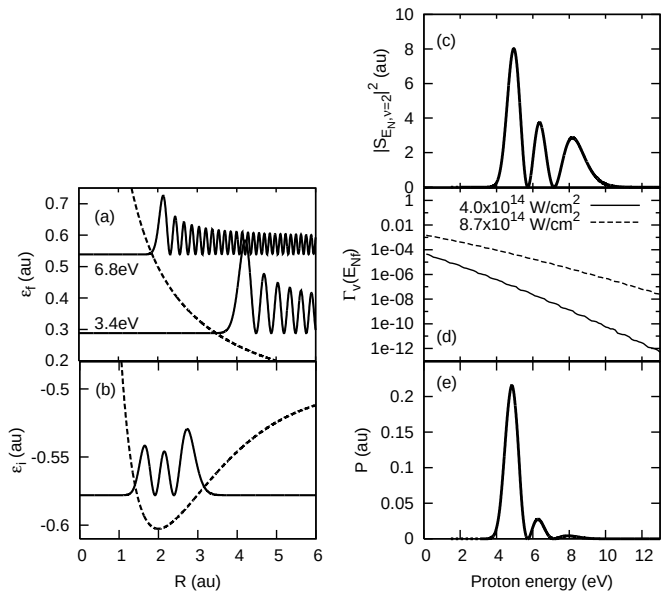

FIG. 2: Calculations showing the result for ions in a vibrational excited initial state with $\nu = 2$. The initial and final wave functions squared are shown in panels (a) and (b). The energies written in panel (a) indicate the proton energy that the particular states correspond to (i.e., one half of the energy of the state). Panel (c) shows the Franck-Condon overlap between the initial vibrational state and the final Coulomb wave for the internuclear coordinate. Panel (d) shows the electronic ionization rate for two different intensities and panel (e) shows the ionization probability using pulses of 45 fs duration (FWHM), 790 nm wavelength and a peak intensity of 8.7×10^{14}W/cm^2, again for ν=2.

used in recent experiments [4, 15]. The spectrum corresponding to a pulse duration of 45 fs and a maximum intensity of 4.1×10^{14} W/cm^2 peaks near 3 eV, while the spectrum is moved to slightly higher energies for pulses with maximum intensity of 8.7×10^{14} W/cm^2. Along with the theoretical predictions, experimental results are also given [4, 15]. The qualitative shape of the distributions is in good agreement in Fig. 1 (c). However, the experimental results at the lower intensity, Fig. 1 (a), show a much broader distribution, with a significant amount of fast protons (energies above 6 eV) not predicted by theory.

To explain the structure of the theoretical spectra we study the contributions from the different initial vibrational states. Since each component contributes incoherently, they can be studied in isolation, and we plot in Figs. 1(b) and (d) these contributions to the overall spectrum. Here we see that even though the molecular ions are predominantly in low vibrational states, the bulk of the Coulomb explosion yield is from highly vibrationally excited states. For pulses of peak intensities near 4.1×10^{14} W/cm^2 ionization from the vibrational states $\nu = 6-11$ is favored, while the $\nu = 4, 5$ and 6 states dominate for pulses of peak intensities near 8.7×10^{14} W/cm^2. It is this shift in origin of the protons that causes the shift in energy of the proton spectrum. Highly vibrationally excited molecular ions contribute to the low energy part of the spectrum, while low-excited molecular ions result in protons of a higher energy.

To see how the structure of the contributions comes about, we examine the initial and final nuclear wave functions. In panel (a) of Fig. 2 the probability densities of two energy-normalized continuum states are presented, along with the density of the $\nu = 2$ state in panel (b). The well known structure of $\nu + 1$ peaks with large probabilities near the classical turning points is seen here. Since we have a continuum of final states which are all peaking at different internuclear separations, this initial structure is reflected in the Franck-Condon overlap $S_{fi\nu}(E_{Nf})$ shown in Fig. 2(c). Remember that large internuclear separations R correspond to low energies. In Fig. 2(d) we show the electronic transition rates for two different intensities. The rates decay, roughly exponentially, with increasing ejected proton energy with an attenuation more pronounced for the higher intensity. When multiplying the Franck-Condon factors and the electronic transition rates and integrating over time we obtain the final result for the $\nu = 2$ case in Fig. 2(e). The influence of the Franck-Condon factor is still apparent but the attenuation produced by the decrease in electronic transition rate suppresses all but the low energies in the proton spectrum. This is reflected in Figs. 1(b) and 1(d), which isolate the contribution of the different vibrational states weighted by their populations. The dominant peak in the contribution is moved towards lower

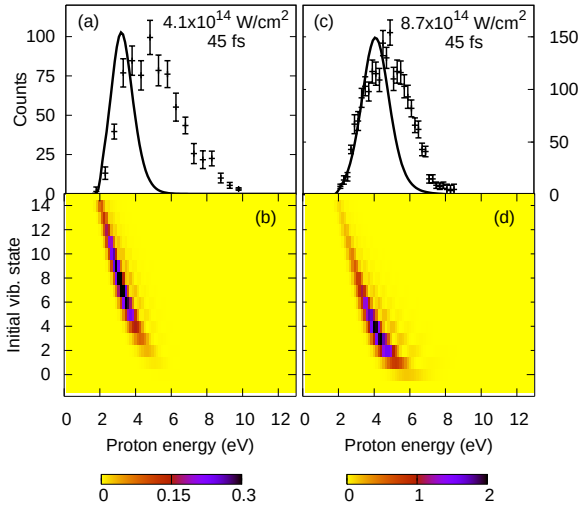

FIG. 3: As Fig. 1, but now using the tunneling theory of Ref. [22].

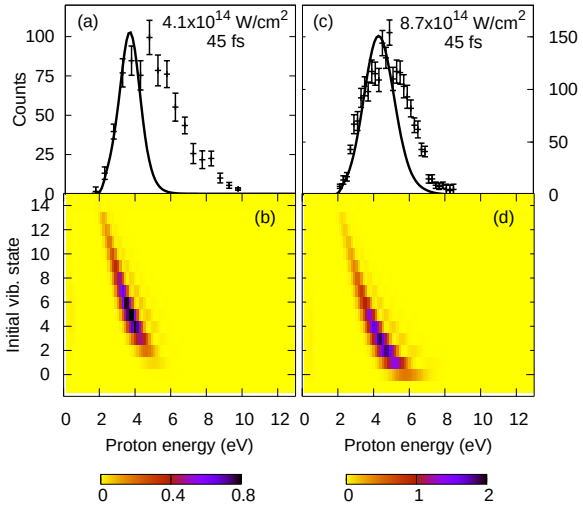

FIG. 4: As Fig. 1, but now using the tunneling theory of Ref. [25].

energies as the molecular ion gets vibrational excited, reflecting the structure of the nuclear wave function showing a classical turning point at a larger nuclear separation.

Comparing Fig. 1(b) and (d) shows that at the higher intensity each vibrational component is broader and the combined spectrum extends to higher energies, which is also expected due to the less rapid decrease of the electronic ionization rate at this intensity. In addition the largest contributions now come from less excited vibrational states. The combination of increase in the high-order multi-photon ionization rate and the relatively larger population in the lower ν states compared to the higher ν states leads to this enhancement of faster protons.

Overall we see a movement of the predicted spectrum towards higher energies as the intensity is raised, both due to the change in the contributions from the different vibrational states and due to the favoring of low excited vibrational states. This tendency is reflected in the measurements, but the resemblance is far from perfect. The lack of agreement may be attributed to several factors. Clearly, a limitation of our model is the calculation of ionization using the strong-field model which is relevant to adiabatic quasi-tunneling. If resonant-enhanced ionization at smaller bond lengths were significant, this would produce faster fragment protons. Also rescattering effects are ignored, which might as well give protons of high energy.

A. Results using tunneling

To complete the discussion of Coulomb explosion of H_2^+ the results using a simple tunneling theory are given. Here the frequency dependence of the field is neglected, and the laser is treated as a slowly-varying (quasi-static) electric field that produces tunneling ionization. Strictly speaking, this static model is only valid when the tunneling time is much shorter than the optical cycle as expressed by $\gamma_K \ll 1$, where $\gamma_K = \sqrt{\frac{I_P}{2U_P}}$ is the Keldysh parameter. For $I = 4.1 \times 10^{14}$W cm^{-2}, $\gamma_K \sim 0.8$, while for $I = 8.7 \times 10^{14}$W cm^{-2}, $\gamma_K \sim 0.5$.

In the tunneling limit the ionization rate at a specific nuclear separation is given as [22]

$$\Gamma_{tun}(R) = \sum_m \left(\frac{3F_0}{\pi\kappa^3}\right)^{\frac{1}{2}} \frac{B^2(m)}{2^{|m|}|m|!} \frac{1}{\kappa^{\frac{2Z}{\kappa}-1}} \left(\frac{2\kappa^3}{F_0}\right)^{\frac{2Z}{\kappa}-|m|-1} \times \exp\left(\frac{-2\kappa^3}{3F_0}\right), \quad (28)$$

where F_0 is the electric field amplitude, $Z = 2$ for H_2^+, $\kappa = \sqrt{2I_p(R)}$ and

$$B(m) = \sum_l C_{l0} D^l_{m0}(R)(-1)^m \sqrt{\frac{(2l+1)(l+|m|)!}{2(l-|m|)!}}. \quad (29)$$

According to [22] the effect of nuclear motion is included by weighting the electronic ionization rate at different internuclear separations with the probability of being at this separation (the reflection principle);

$$\frac{dw}{dR} = \Gamma_{tun}(R)|\chi_i(R)|^2. \quad (30)$$

This result can be translated into a function of the proton kinetic energy by assuming that all the Coulomb energy between the two protons at the time of ionization is translated into proton ejection energy. The results are shown in Fig. 3.

Compared to the strong-field approximation model the low energy part of the spectrum shows better agreement with experiments, but the high-energy part is again

poorly represented. The reason for the better agreement in the low-energy part of the spectrum is clear from Figs. 3(b) and (d): a shift towards lower vibrational states and an exponential favoring of the low energy part of the spectrum as is typical for a tunneling theory. The lack of agreement at high proton energy could be an indication that multiphoton resonance ionization is involved at smaller bond lengths, and this is clearly absent within the static field tunneling model.

Another way of using tunneling theory to describe Coulomb explosion of H_2^+ is to include the effect of nuclear motion as described in Ref. [25]. The overall rate is here found by

$$\frac{dw}{dE_{Nf}} = \left| \int \chi_f(R) \Gamma_{tun}^{\frac{1}{2}}(R) \chi_i(R) dR \right|^2 . \qquad (31)$$

The results are given in Fig. 4, and show an even larger shift towards lower vibrational excited states resulting in a slightly better agreement particularly for the high intensity case.

IV. CONCLUSION

In this work we have presented a relatively simple quantum mechanical model to describe Coulomb explosion of molecular hydrogen ions. The model builds on the length gauge molecular strong-field approximation and gives reasonable predictions when compared with experiment. Theory predicts a dominant proton emission at slightly lower energies than the experimental measurements. However, the effect of multiphoton resonance ionization contributions, known to be significant for this range of intensities, could be important.

The strong-field approximation allows very simple and fast calculations and might, for that reason, be a useful tool in the further understanding of molecular dynamics, including related intense field processes as, e.g., high-harmonic generation. For all purposes it is important only to use the model in the regime, where it is valid, namely describing pulses of high intensities and short durations. If the pulse duration exceeds 50 fs the molecular ion will have time to dissociate and the resulting KER-spectrum will move to considerably lower energies.

For comparison we have discussed the predictions from two different tunneling models. The spectrum is here somewhat narrower and also centered near to low energies.

Acknowledgments

We thank Thomas Kim Kjeldsen for useful discussions. L.B.M. thanks Xavier Urbain for discussions on the distribution over vibrational levels and the University of Louvain-La-Neuve for hospitality and support. The present work was supported by the Danish Research Agency (Grant. No. 2117-05-0081).

[1] A. Giusti-Suzor, F. H. Mies, L. F. DiMauro, E. Charron, and B. Yang, Journal of Physics B: Atomic, Molecular and Optical Physics **28**, 309 (1995), URL http://stacks.iop.org/0953-4075/28/309.

[2] J. H. Posthumus, Reports on Progress in Physics **67**, 623 (2004), URL http://stacks.iop.org/0034-4885/67/623.

[3] J. F. McCann and J. H. Posthumus, Philosophical Transactions of the Royal Society A: Mathematical, Physical and Engineering Sciences **357**, 1309 (1999), URL http://dx.doi.org/10.1098/rsta.1999.0376.

[4] I. Ben-Itzhak, P. Q. Wang, J. F. Xia, A. M. Sayler, M. A. Smith, K. D. Carnes, and B. D. Esry, Physical Review Letters **95**, 073002 (pages 4) (2005), URL http://link.aps.org/abstract/PRL/v95/e073002.

[5] K. C. Kulander, F. H. Mies, and K. J. Schafer, Phys. Rev. A **53**, 2562 (1996).

[6] D. Pavicic, Ph.D. thesis, Max Planck Institute of Quantum Optics (2004).

[7] D. Pavicic, A. Kiess, T. W. Hnsch, and H. Figger, The European Physical Journal D - Atomic, Molecular, Optical and Plasma Physics **26**, 39 (2003), URL http://dx.doi.org/10.1140/epjd/e2003-00197-2.

[8] D. Pavicic, A. Kiess, T. W. Hansch, and H. Figger, Physical Review Letters **94**, 163002 (pages 4) (2005), URL http://link.aps.org/abstract/PRL/v94/e163002.

[9] T. Zuo and A. D. Bandrauk, Phys. Rev. A **52**, R2511 (1995).

[10] L.-Y. Peng, D. Dundas, J. F. McCann, K. T. Taylor, and I. D. Williams, Journal of Physics B: Atomic, Molecular and Optical Physics **36**, L295 (2003), URL http://stacks.iop.org/0953-4075/36/L295.

[11] I. Ben-Itzhak, P. Wang, J. Xia, A. M. Sayler, M. A. Smith, J. Maseberg, K. D. Carnes, and B. D. Esry, Nuclear Instruments and Methods in Physics Research Section B: Beam Interactions with Materials and Atoms **233**, 56 (2005), URL http://www.sciencedirect.com/science/article/B6TJN-4G1R3H9-

[12] T. Ergler, A. Rudenko, B. Feuerstein, K. Zrost, C. D. Schröter, R. Moshammer, and J. Ullrich, Journal of Physics B: Atomic, Molecular and Optical Physics **39**, S493 (2006), URL http://stacks.iop.org/0953-4075/39/S493.

[13] S. Saugout and C. Cornaggia, Physical Review A (Atomic, Molecular, and Optical Physics) **73**, 041406 (pages 4) (2006), URL http://link.aps.org/abstract/PRA/v73/e041406.

[14] J. McKenna, W. A. Bryan, C. R. Calvert, E. M. L. English, J. Wood, D. S. Murphy, I. C. E. Turcu, J. M. Smith, K. Ertel, O. Chekhlov, et al., Journal of Modern Optics **in press** (2007).

[15] B. D. Esry, A. M. Sayler, P. Q. Wang, K. D. Carnes, and I. Ben-Itzhak, Physical Review Letters **97**, 013003 (pages 4) (2006), URL

http://link.aps.org/abstract/PRL/v97/e013003.

[16] T. K. Kjeldsen and L. B. Madsen, Journal of Physics B: Atomic, Molecular and Optical Physics **37**, 2033 (2004), URL http://stacks.iop.org/0953-4075/37/2033.

[17] T. K. Kjeldsen and L. B. Madsen, Physical Review A (Atomic, Molecular, and Optical Physics) **71**, 023411 (pages 10) (2005), URL http://link.aps.org/abstract/PRA/v71/e023411.

[18] L.-Y. Peng, I. D. Williams, and J. F. McCann, Journal of Physics B: Atomic, Molecular and Optical Physics **38**, 1727 (2005), URL http://stacks.iop.org/0953-4075/38/1727.

[19] D.M. Brink and G.R. Satchler, *Angular Momentum* (Oxford University Press, London, 1968); R.N. Zare, *Angular Momentum* (Wiley, New York, 1988).

[20] G. F. Gribakin and M. Y. Kuchiev, Phys. Rev. A **55**, 3760 (1997).

[21] T.K. Kjelsden, C.Z. Bisgaard, L.B. Madsen, and H. Stapelfeldt, Phys. Rev. A **71**, 013418 (2005).

[22] X. M. Tong, Z. X. Zhao, and C. D. Lin, Phys. Rev. A **66**, 033402 (2002).

[23] I. S. Gradshteyn and I. M. Ryzhik, *Table of Integrals, Series, and Products* (Academic Press, San Diego, 1994).

[24] H. Niikura, F. Lgar, R. Hasbani, A. D. Bandrauk, M. Y. Ivanov, D. M. Villeneuve, and P. B. Corkum, Nature **417**, 917 (2002).

[25] X. Urbain, B. Fabre, E. M. Staicu-Casagrande, N. de Ruette, V. M. Andrianarijaona, J. Jureta, J. H. Posthumus, A. Saenz, E. Baldit, and C. Cornaggia, Physical Review Letters **92**, 163004 (pages 4) (2004), URL http://link.aps.org/abstract/PRL/v92/e163004.